tvst

https://doi.org/10.1167/tvst.8.3.61

Article

First Clinical Application of Low-Cost OCT

Ge Song[1], Kengyeh K. Chu[1], Sanghoon Kim[1], Michael Crose[1], Brian Cox[1], Evan T. Jelly[1], J. Niklas Ulrich[2], and Adam Wax[1]

[1] Department of Biomedical Engineering, Duke University, Durham, NC, USA
[2] Kittner Eye Center, University of North Carolina, Chapel Hill, NC, USA

Correspondence: Adam Wax, Department of Biomedical Engineering, Duke University, Durham, NC 27708, USA. e-mail: a.wax@duke.edu

Received: 12 March 2019
Accepted: 7 May 2019
Published: 28 June 2019

Keywords: diagnostic imaging; point of care; optical coherence tomography

Citation: Song G, Chu KK, Kim S, Crose M, Cox B, Jelly ET, Ulrich JN, Wax A. First clinical application of low-cost OCT. Trans Vis Sci Tech. 2019;8(3):61, https://doi.org/10.1167/tvst.8.3.61
Copyright 2019 The Authors

Purpose: We present the design of a new low-cost optical coherence tomography (OCT) system and compare its retinal imaging capabilities to a standard commercial system through a clinical study.

Methods: A spectral-domain OCT system was designed using various cost-reduction techniques to be low-cost, highly portable, and completely stand-alone. Clinical imaging was performed on 120 eyes of 60 patients (60 eyes of normal volunteers and 60 eyes with retinal disease) using both the low-cost OCT and a Heidelberg Engineering Spectralis OCT. Contrast-to-noise ratio (CNR) was measured from resulting images to determine system performance.

Results: The low-cost OCT system was successfully applied to clinical imaging of the retina. The system offers an axial resolution of 8.0 μm, a lateral resolution of 19.6 μm, and an imaging depth of 2.7 mm for a 6.6-mm field of view in the X and Y directions. Total cost is $5037, a significant size reduction compared to current commercial higher performance systems. Mean CNR value of low-cost OCT images is only 5.6% lower compared to the Heidelberg Spectralis.

Conclusions: The images captured with the low-cost OCT were of adequate resolution and allowed for clinical diagnostics. It offers comparable performance as a retinal screening tool at a fraction of the cost of current commercial systems.

Translational Relevance: Low-cost OCT has the potential to increase access to retinal imaging.

Introduction

Spectral-domain optical coherence tomography (SD-OCT) is currently recognized as the gold standard for identifying structural retinal abnormalities in ophthalmology. Due to its ability to acquire fast, highly sensitive in vivo cross-sectional images of the histologic layers of the retina, OCT is an excellent screening tool to use to detect retinal pathology.[1,2] For retinal diseases, early detection via regular patient screening can be crucial in introducing treatment before potentially permanent vision loss occurs.[3] OCT is particularly useful as a screening tool, both for early detection of disease and to follow treatment success.

Recently, development of handheld OCT probes has accelerated, driven by increased commercial availability of miniaturized optics and the need for the flexibility of manual manipulation in many clinical applications.[4] Various scanning-based handheld OCT probes have been demonstrated for a wide range of applications, such as inner ear imaging,[4] retinal angiography,[5] elastography,[6] and with combined modalities.[7] Typically, handheld probes enclose the OCT scanner arm within a manufactured housing.[8] A scanning element such as a microelectromechanical system (MEMS) mirror or galvanometer-based scanner placed in the sample arm allow 2D cross-sections or 3D volumes to be acquired.[9,10] Though such systems enable greater flexibility for clinical imaging, they are partitioned into a lightweight handheld unit that interfaces with the patient or sample and a base unit that contains most of the OCT imaging instrumentation. One barrier to more widespread OCT screening is system portability and size. Portability is typically limited by the bulk of the base unit, which must house the reference arm,

This work is licensed under a Creative Commons Attribution-NonCommercial-NoDerivatives 4.0 International License.

Downloaded from abstracts.iovs.org on 04/24/2024

spectrometer, broadband light source, computer, and display. While these units can be made transportable by installing them into a wheeled enclosure, they remain significantly less portable than the handheld scanner itself. One of the goals of our present work was to significantly improve the portability of the base unit to which the handheld probe is tethered so that the complete instrument can be easily moved and stored; this we were able to accomplish by placing the entire interferometer within the handheld probe and reducing the size of the spectrometer, computer, and display.

Another limitation of current OCT systems is high cost, which is reflected in studies of patient-screening rates. In the United States, diseases such as diabetic retinopathy have become the leading causes of blindness among the adult population.[11] For Americans 40 years and older with diabetes, 28.5% are affected by diabetic retinopathy and 4.4% suffer from vision-threatening diabetic retinopathy.[12] The American Academy of Ophthalmology recommends routine eye examinations to screen diabetic patients, often at the time of diagnosis and at least annually afterward.[13,14] A recent data study of 298,383 insured diabetic patients in the United States reveals that nearly half of them had no eye exam visits over a 5-year period, while only 15.3% met the recommendation for annual or biennial eye exams.[15] This is particularly unfortunate for patients in underserved environments, where routine eye screening is often limited and even unavailable. For ethnic and racial minorities with diabetes, the annual screening rate can be significantly lower: between 33% to 45% for African Americans and Hispanics over a 1- to 2-year period,[16,17] with one study showing 63% of its patients having had no eye exams for more than 2 years.[18] Patients in these populations often lack the means of transportation and access to a nearby eye clinic that offers screening. As a result, blindness from diabetic retinopathy is two times more likely in minority populations.[19] While OCT screening in addition to standard dilated fundus exams is desirable, current commercial systems remain bulky and high in cost; their availability can be limited outside of larger eye clinics, hospitals, and research laboratories.[20] A need, therefore, remains for a low-cost OCT system that is readily accessible to perform clinical screening. For point-of-care diagnostics, an OCT system should be portable and low cost, while still maintaining the necessary sensitivity and contrast offered by a high-performance system. Furthermore, the usability of a low-cost OCT depends on the ease of use of the device, as well as its ability to store patient data to be readily transferred for expert review.

Here we present a new low-cost OCT system and evaluate its performance against another commercial system in a clinical setting. We previously introduced the design for a low-cost OCT based on a custom spectrometer design and off-the-shelf parts and development kits.[21] To adapt this design for clinical application, we redesigned several components. The system topology was changed to incorporate several of the optical components into a 3D-printed handheld scanner to improve portability while also increasing system robustness. Furthermore, the portability and form factor of the system were improved by incorporating a 7-inch thin film transistor (TFT) touchscreen into the system housing to allow direct clinician interaction for image acquisition. Further cost reduction was achieved through the incorporation of a non–temperature-controlled superluminescent diode (SLD), a custom-designed spectrometer, and completely custom-designed control circuit boards. Through these changes, the total cost of materials was lowered to $5037, which was 80% to 90% less costly than current commercial OCT machines. To demonstrate the clinical applicability of the low-cost OCT, we conducted a clinical study to evaluate its imaging capabilities. Images taken with the low-cost OCT were compared to those acquired by a standard commercial system. Through standard image quality metric analysis, we aimed to show the potential of the low-cost OCT system as a useful tool for point-of-care diagnostics.

Methods

The low-cost OCT is based on a Michelson low-coherence interferometer setup (Fig. 1), consisting of four arms from a 50:50 fiber optic coupler: one from the light source, which is split by the coupler into the reference arm and sample arm. Light returning from both arms is recombined at the splitter and sent to the spectrometer for detections. The handheld scanner was designed to house the light source, reference arm, and sample arm, which greatly reduced the size of the OCT system body. The custom-designed spectrometer was housed inside a 3D-printed system body, along with an integrated mini-PC. To allow complete stand-alone operation of the system, a 7-inch TFT touchscreen was incorporated into the system body to allow controls for data acquisition and display of retinal images. Multiple printed circuit control boards

Downloaded from abstracts.iovs.org on 04/24/2024

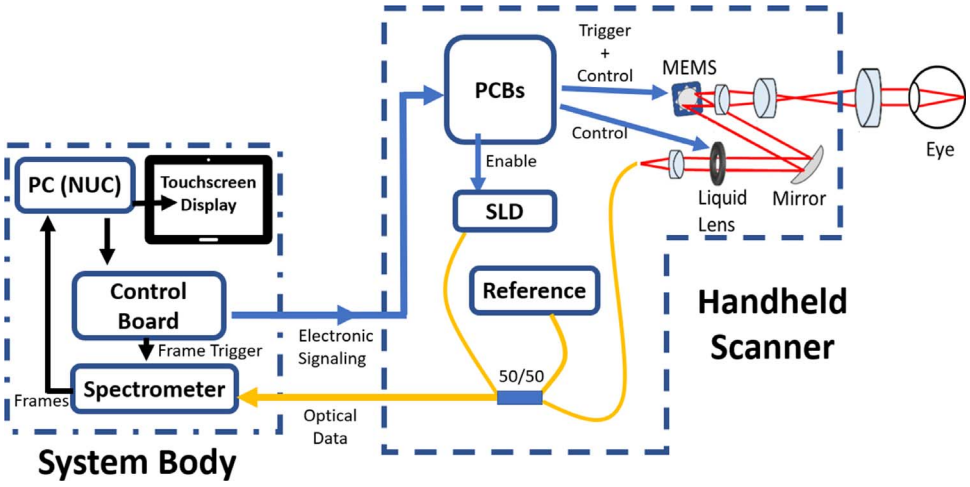

Figure 1. System block diagram illustrating the system body, which consists of the spectrometer, PC, touchscreen, and printed control board, and the handheld scanner, which contains the optics of the Michelson interferometer along with control electronics and scanning elements.

were custom designed to synchronize the scanning and frame acquisition during imaging. Functions of these boards include current supply of the superluminescent light source, one to control the scanning elements (MEMS, liquid lens), one for the spectrometer sensor and control, and a master controller board to serve as a timing generator. The use of these boards significantly reduced the cost of the overall system; their individual functions are described later in more detail.

Interferometer

The light source for the low-cost system was a fiber pigtailed SLD with open-loop thermoelectric cooling (SLD, 3.5 mW, Exalos BTF14; Exalos AG, Schlieren, Switzerland). The fiber optic output from this source was fusion spliced to one of the arms of a 50:50 fiber coupler (TN830R5A2; Thorlabs, Inc., Newton, NJ). The SLD was measured to have a center wavelength of 830 nm and a full width at a half maximum bandwidth of 42 nm. The spectrometer was based on our previous design,[21] containing a parabolic mirror, a fold mirror, a transmission diffraction grating (T-1850-800s; LightSmyth Technologies, Inc., Eugene, OR), and two stacked 150-mm focal length achromatic doublets (AC254-150-B; Thorlabs) in a loop configuration. A tall pixel CMOS sensor array consisting of 2048 pixels was used as the detector (S11639-01; Hamamatsu, Hamamatsu City, Japan), although only half of the array was utilized in order to increase A-scan line rate. The reference arm optics were housed into an adjustable-length lens tube to enable pathlength adjustments to match that of the sample arm.

The scanner optics were designed using software (OpticStudio; Zemax, LLC, Kirkland, WA) to achieve a longer working distance than our previous implementation (Fig. 2). A working distance of 17.5 mm was implemented to avoid accidental contact between the objective and the patient's eye or eyelash during imaging. In addition to a longer working distance, the design maintains a sufficient field of view (FOV) of 6.6 mm and a spot size less than 20 μm on the retina, which is beneficial for clinical imaging. The scanning mechanism is based on a MEMS mirror (A7B2.1-3600AL; Mirrorcle Technologies Inc., Richmond, CA) and a liquid lens (Optotune, Dietikon, Switzerland). This combination allowed for independent scanning and dynamic focusing control to achieve the optimal spot size for a given patient with this system. The use of the liquid lens enabled focusing at multiple depths without having to adjust imaging optics, allowing accommodation for different patients.

Synchronization and Software

The OCT software is a custom Windows application (Microsoft Visual Studio; Microsoft, Redmond, WA) written in C# and C++. The user interface is displayed on the integrated touchscreen to allow system control and interaction by a clinician (Fig. 3). The interface is configured to enable patient demographic input, scanning direction selection, and focus control. Once an image is acquired, the last 30 frames

Downloaded from abstracts.iovs.org on 04/24/2024

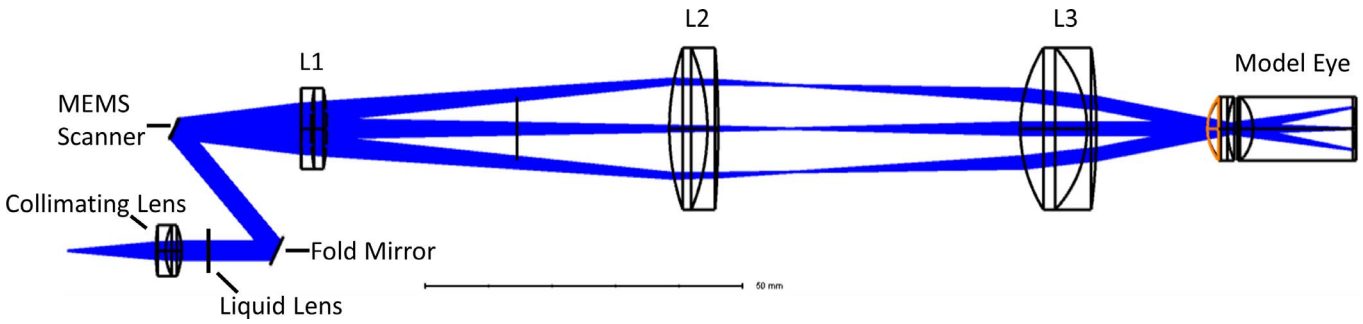

Figure 2. Scanner arm design illustrating the liquid lens and MEMS scanner, including a model human eye to analyze optical performance.

are retained in the buffer, allowing the operator to review them before saving both the processed and raw B-scans on the hard drive of the integrated PC. Using the current custom-designed control board, an A-scan rate of 12.5 kHz is achieved.

Synchronization between the scanner optics and the sensor array is effected by the master controller board in the main system body, which sends a trigger signal to the MEMS control board in the handheld scanner to begin each lateral scan. The MEMS control board contains a digital-to-analog converter to generate an analog voltage that is amplified through a high-voltage rail to implement movement of the MEMS mirror. Once scanning begins, the master controller board sends a frame trigger command to the spectrometer to begin acquiring A-scans. The spectrometer board consists of a daughter board to interface to the sensor and a board to digitize and send signals (B-scans) back to the PC through the USB 3.0 port. The PC receives and processes the frames before displaying images on the touchscreen through HDMI. Focusing was adjusted through the microcontroller on the scanner board, which alters the current through the liquid lens,

Figure 3. Low-cost OCT user interface displaying a healthy retina during clinical imaging. To ensure functionality and ease of access during imaging, a simplified interface that adapts to the 7-inch touchscreen was used. The main tab is where patient data, eye, and scan direction can be inputted. The clinician presses "Start Scan" to begin imaging the retina. Review tab is where the clinician can review the last 30 frames before saving both raw and processed B-scans.

Downloaded from abstracts.iovs.org on 04/24/2024

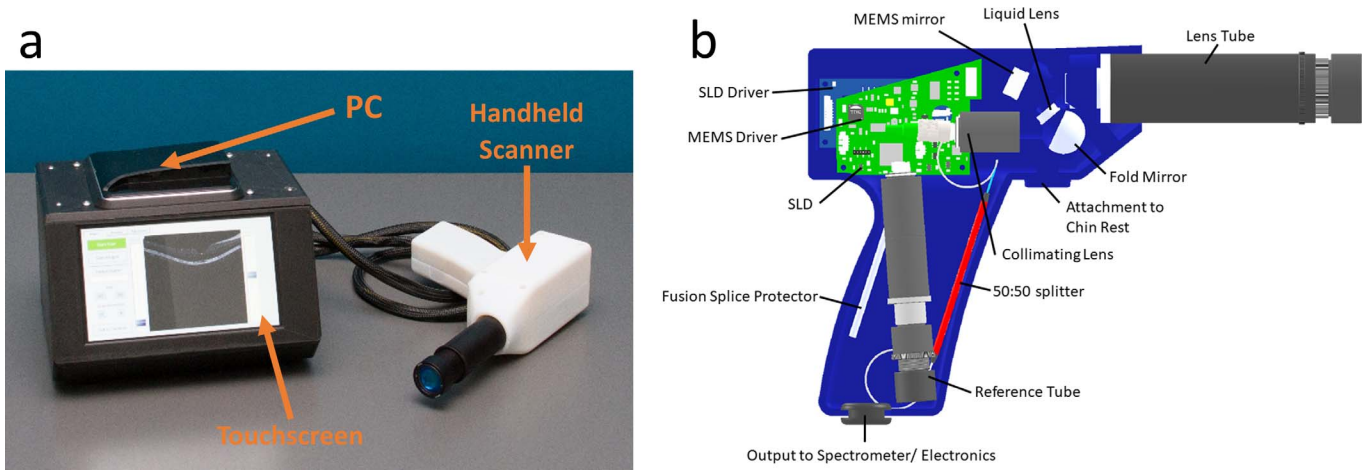

Figure 4. (a) Complete low-cost OCT system showing PC, touchscreen, and scanner. (b) Detailed composition inside the low-cost OCT handheld scanner.

shaping its spherical contour electrically. The master controller board communicates to the SLD board through a serial peripheral interface, which sets the current needed to drive the light source.

Optical Assembly

Both the system body and the handheld scanner housing were fabricated using 3D-printing technology (3D45; Dremel, Mount Prospect, IL, and Connex3 Objet350; Stratasys, Eden Prairie, MN, respectively). The use of 3D-printed parts allows the low-cost OCT to be more compact and lightweight in contrast to machined aluminum parts used in most commercial systems. Both the mini-PC (NUC515RYK; Intel Corp., Santa Clara, CA) and the touchscreen (Newhaven Display International, Inc., Elgin, IL) were mounted in the system body to allow easy user access to software and the PC's USB ports. The fiber interferometer optics and printed circuit boards are contained in the scanner housing. This offers a significant advantage in that manipulation of the handheld scanner does not change the polarization state of the reference arm light relative to that in the sample arm since the two signals are combined prior to directing to the spectrometer. Polarization of the light in the two arms was optimized through geometric manipulation of the optical fibers before they were fixed into place in the scanner housing. For design of this component, key inputs for clinical ease of use were limiting handheld scanner size and weight, and thus they were prioritized in the final system (Fig. 4). Lastly, the handheld scanner was made to easily attach to a standard slit lamp chin rest as is typically available in eye clinics to allow maximum control and stability during retinal imaging.

Imaging Protocol

To demonstrate the clinical capabilities of the low-cost system, retinal imaging was performed at the University of North Carolina Kittner Eye Center (Institutional Review Board, Study no. 17-2094). One hundred twenty eyes of 60 patients (36 female and 24 male) were imaged using the low-cost OCT system as well as the standard Heidelberg Spectralis OCT (Heidelberg Engineering GmbH, Heidelberg, Germany). Out of the 120 eyes imaged, 60 were eyes of healthy volunteers, while the other 60 had known retinal pathology. Healthy subjects had an age range between 20 and 60 years, and patients with retinal pathology had a mean age of 70.4 years. Written consents from all 60 patients were obtained prior to the study, and imaging was performed by an on-site expert. Subjects with retinal pathology were dilated for OCT imaging, since dilation was part of the standard of care for their same-day regular ophthalmic screening. Imaging on the Heidelberg Spectralis was performed according to standard protocol at the Kittner Eye Center. For low-cost OCT imaging, each subject was seated on a chair facing the operator (Fig. 5). The low-cost OCT system was placed on a table between the operator and the subject. Although it is designed to be operable as a handheld device, the low-cost scanner was mounted on a chin rest to ensure a degree of stability comparable to the Spectralis device. The use of the chin rest also decreases imaging time so as to not interfere with the workflow of the clinical site. Each subject was told to fixate on the scanning

Downloaded from abstracts.iovs.org on 04/24/2024

Figure 5. On-site ophthalmic photographer performs imaging of a patient using the low-cost OCT at the UNC Kittner Eye Center.

OCT beam, which appears as a red line during imaging, while the operator controlled the scanner position and observed the B-scans in real time on the touchscreen. The operator positioned the scanner manually to achieve the best image and electronically controlled focus using the touchscreen to maximize signal from the retina. Once the operator was satisfied with an acquired image, the software permitted a review of the last 30 frames captured before saving both the raw and processed B-scans. Each subject was scanned four times total with both the low-cost OCT and the Heidelberg Spectralis (one horizontal and one vertical scan in each eye). Images acquired from the Heidelberg Spectralis were set to two-frame averages, which is the lowest frame option allowed on the device. Low-cost OCT acquisitions were single frame B-scans, with two-frame average applied in post-processing for fair comparison. Although the low-cost OCT system already saves processed B-scans, raw B-scans were also saved to permit subsequent image metric analysis.

To demonstrate the ability of the system to acquire retinal images without the chin rest and frame, we imaged five patients with healthy retinas within the study using the scanner manually held in free space. To image in handheld mode, an operator placed one hand on the face of the patient, allowing the tip of the scanner optics to rest on the thumb, while manipulating the scanner with the other hand.

Image Metric Analysis

Automated quantitative analysis was performed to compare the quality of the images acquired by the low-cost OCT to those acquired by the Heidelberg Spectralis (Fig. 6). Raw B-scan data were processed using standard SD-OCT methods, with an additional speckle reduction method applied.[22,23] To alleviate the effect of interframe motion, two sequential images from the low-cost OCT system were horizontally and vertically pixel-shifted to maximize the 2D cross-correlation coefficient between consecutive frames prior to two-frame averaging, matching the two-frame minimum averaging performed automatically by the Heidelberg Spectralis system. Upon inspecting the pixel intensity distributions of images from both devices, it was apparent that the Heidelberg Spectralis system images exhibited a different distribution of pixel intensities, which is near-Gaussian in many cases, as compared to that from the low-cost OCT system, which showed a Rayleigh distribution. Therefore, to enable a fair comparison between the two systems, a histogram-matching procedure was devised and applied to the corresponding low-cost OCT images as part of the automatic-processing procedure. The matching function was generated by fitting the intensity histogram for each Heidelberg Spectralis image using a third-order polynomial and

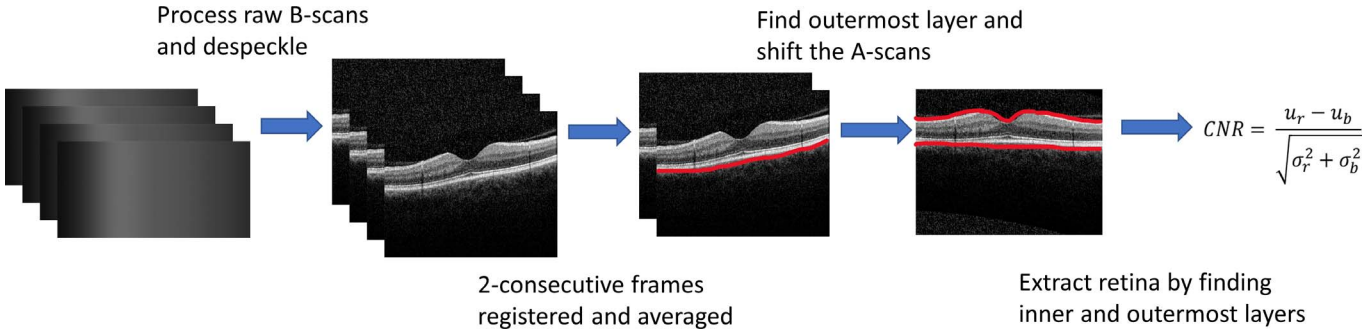

Figure 6. Image analysis steps taken to extract values needed to perform CNR calculations for images taken from the low-cost OCT. For images taken on the Heidelberg Spectralis, only the flattening and retina extraction steps needed to be performed.

Downloaded from abstracts.iovs.org on 04/24/2024

applied to equalize the corresponding pixel intensities for the images acquired by the low-cost OCT. Finally, both the low-cost OCT images and the Heidelberg Spectralis images were vertically shifted column by column to present a horizontal retinal orientation. This was to account for some images captured from both devices that showed the retinas tilted across the FOV as a result of subject eye movements. The flattening was performed by identifying the outermost layer of the retina and vertically shifting each A-scan in the image with respect to that layer. Images acquired on the low-cost OCT using handheld mode were processed in the same manner.

A metric commonly used to analyze OCT image contrast is the contrast-to-noise ratio (CNR).[24] For logarithmic OCT images, CNR is represented by

$$\mathrm{CNR} = \frac{u_r - u_b}{\sqrt{\sigma_r^2 + \sigma_b^2}}, \quad (1)$$

where u_r and σ_r are the mean and standard deviation of region of interest, respectively, and u_b and σ_b are the mean and standard deviation of the background noise, respectively. The region of interest in this case was the entire retina, which was extracted from each image by taking the values between the inner and outermost layers of the retina using an edge-detection method. After the region of interest was defined, the CNR was calculated for each image.

Results

System Performance

Through various cost-reduction designs and custom fabrication of key system components, the complete OCT system was manufactured for a total parts cost of $5037. The complete table of costs is shown in Table 1, which breaks down the parts within the system, such as the spectrometer and handheld scanner. Exact costs of 3D printing and electronics are also provided.

The current low-cost OCT system demonstrated an axial resolution of 8.0 μm, a lateral resolution of 19.6 μm, and an imaging depth of 2.7 mm for a 6.6-mm FOV in the X and Y directions. The weight of the system body is 1.8 kg, and the weight of the handheld scanner is less than 500 g, for a total system weight of 2.3 kg. System specifications and comparison to the Heidelberg Spectralis are presented in Table 2. The output scanner power ranged from 400 to 680 μW. This was due to the use of a non–temperature-controlled SLD, which suffered from power fluctuations. Although continuous background subtraction was performed during imaging to reduce common path artifacts, the SLD power fluctuations did affect the resulting contrast of the images, which we discuss later.

Table 1. Complete List of Costs for Low-Cost OCT System

Item	Cost, $
Spectrometer	
Sensor and boards	260
Lenses and tubes	234
Grating	245
Grating mount	275
Folding mirrors	375
Subtotal	1389
Optical Components	
SLD	500
Optical fiber	120
Fiber splitter	242
Reference arm	273
Connectors	18
Subtotal	1153
3D Printing	
Scanner mount	4
System body housing	12
Scanner housing	118
Spectrometer housing	6
Subtotal	140
Scanner	
MEMS mirror	635
Liquid lens	102
Lenses and mirrors	311
Tubes and adapter	104
Subtotal	1152
Electronics	
PC and accessories (USB and HDMI cables)	750
Controller board	50
Scanner board	104
SLD driver board	36
Touchscreen	115
Subtotal	1055
Misc. assembly parts (screws and cables)	148
Total	5037

Figures 7 and 8 show images acquired using both the low-cost OCT and the Heidelberg Spectralis systems from normal, healthy subjects. The low-cost OCT images can clearly resolve relevant layers of the

Downloaded from abstracts.iovs.org on 04/24/2024

Table 2. Low-Cost OCT and Heidelberg Spectralis Optical System Performance

Parameter	Low-Cost OCT	Heidelberg Spectralis
Center wavelength, nm	830	870
Bandwidth, nm	42	N/A
Number of pixels per A-scan	512	512
Scanner output power	400–680 μW	1.2–1.3 mW
Imaging depth, mm	2.7	1.8
Axial resolution, μm	8.0	7.0
Lateral resolution, μm	19.6	14
A-scan rate, kHz	12.5	40
Sensitivity, dB	104	N/A
Working distance, mm	17.5	7–15(estimated)
Scan range (X and Y), mm	6.6	9
Weight, kg		
With PC	1.8	
Without PC		27.6
Volume, in^3	250	3590
Cost, $	5037	>60,000

N/A indicates parameter was not available.

retina, comparable to the images from the Heidelberg Spectralis system. In comparison to the Heidelberg system images, which have a stronger retina signal from a higher incident optical power, the low-cost OCT images appear lower in intensity. However, the low-cost OCT images exhibit more uniform and lower background noise variance in comparison to the Heidelberg system images. Notably, the Heidelberg system images show a step function–like noise variance, where there are large noise variances in the region above the retina, followed by three- to four-fold lower noise variances at regions beneath the outer segments of the retina.

Similarly, retinal images from patients with known pathologies are shown for four patient cases for both the Heidelberg and the low-cost OCT systems. Figure 9 (top left) shows images of a patient with macular puckering. An epiretinal membrane causes wrinkling of the inner retina and an absent foveal depression. Figure 9 (bottom left) shows multiple drusenoid pigment epithelial detachments in a patient with age-related macular degeneration. Image pairs on the right of Figure 9 both demonstrate intraretinal cysts and hard exudates in patients with diabetic macular edema.

A paired *t*-test was performed using statistical software (JMP Pro; SAS, Cary, NC) to compare the CNR of the images from the low-cost OCT and Heidelberg systems. A few images that inadvertently had an incorrect setting for frame average on the Heidelberg system were excluded from analysis. The corresponding low-cost images, therefore, were also excluded. CNR value distributions for images from both the Heidelberg and the low-cost OCT system follow Gaussian distributions and pass corresponding normality tests ($P > 0.05$). A Grubbs test was performed to eliminate any outliers in CNR values. However, due to the large sample size of image CNR values, the presence of a few outliers did not have a significant effect on the resulting comparison. Without distinguishing between normal and pathology groups, the low-cost OCT demonstrated a mean CNR value of 1.592 ± 0.021, while that of the Heidelberg Spectralis was 1.687 ± 0.027. The paired *t*-test supported the 5.6% difference in mean CNR as statistically significant between images acquired by the low-cost OCT and those acquired by the Heidelberg Spectralis ($P < 0.0001$). A similar difference exists between the two devices when comparing pathology-only images (5.3%, $P = 0.0004$) as well as comparing normal-only images (6.0%, $P < 0.0001$). CNR distributions and statistical analysis are summarized in Figure 10 and Table 3.

We were also able to obtain high-quality images with an operator hand holding the scanner without a chin rest; a representative image is shown in Figure 11. To determine if the image quality obtained during freehand acquisitions differed significantly from the images acquired using a chin rest, we performed a paired *t*-test on the difference of CNR between the

Downloaded from abstracts.iovs.org on 04/24/2024

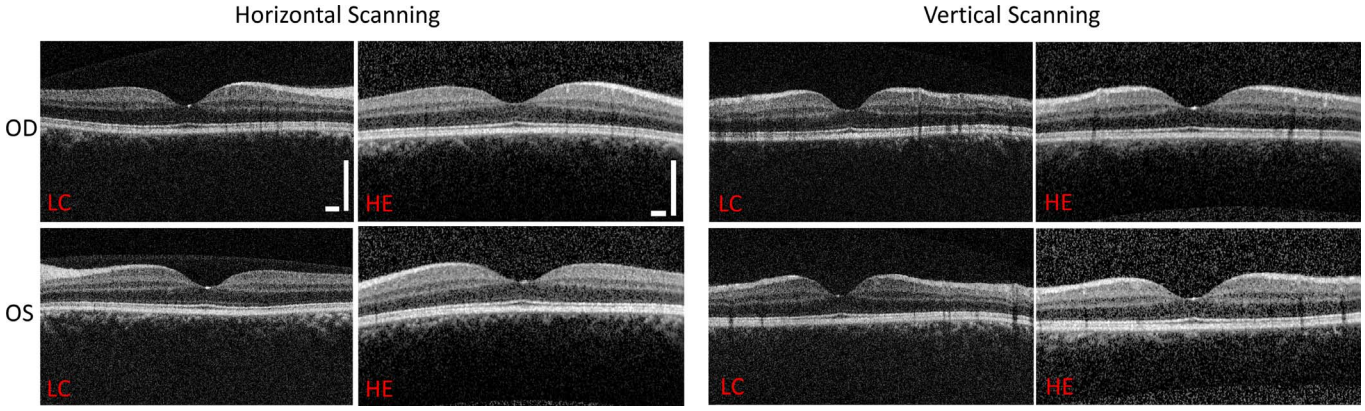

Figure 7. Side-by-side comparisons of low-cost OCT system images and Heidelberg system images for a single patient. OD, right eye; OS, left eye; LC, low cost; HE, Heidelberg Engineering. *Scale bars*: 500 μm.

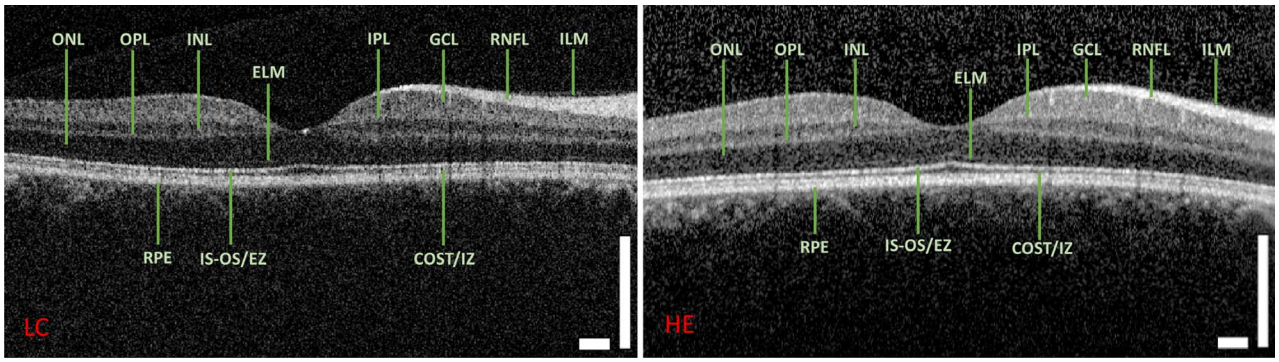

Figure 8. Images of the right eye from a healthy patient acquired using the low-cost OCT and Heidelberg Spectralis systems. RNFL, retinal nerve fiber layer; GCL, ganglion cell layer; IPL, inner plexiform layer; INL, inner nuclear layer; OPL, outer plexiform layer; ONL, outer nuclear layer; ELM, external limiting membrane; IS-OS/EZ, inner segment/outer segment junction line; COST/IZ, cones outer segment tips line/interdigitation zone; RPE, retinal pigmented epithelium. *Scale bars*: 500 μm.

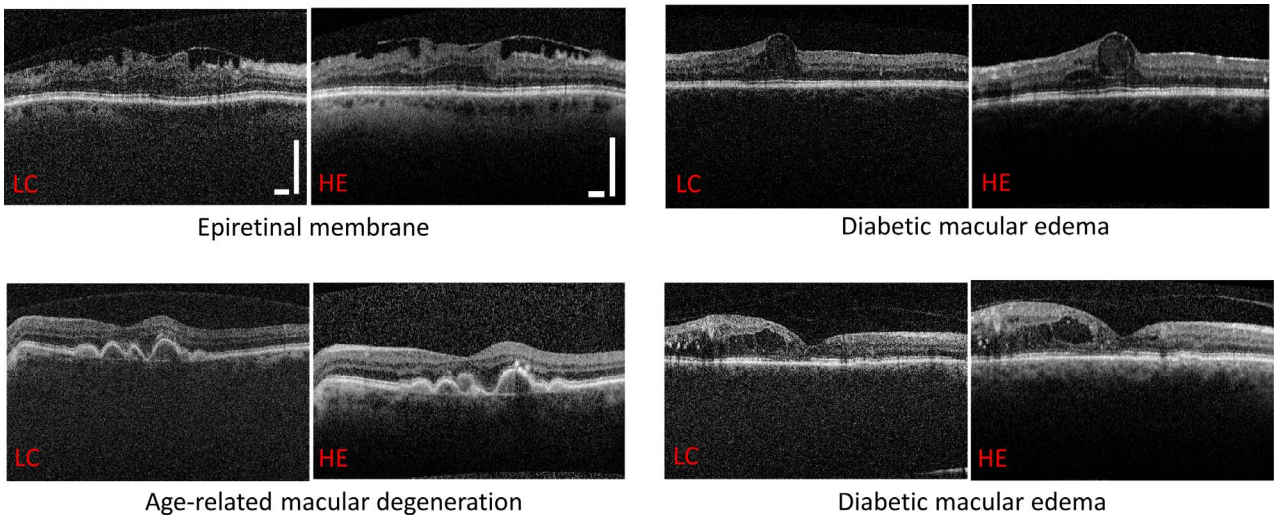

Figure 9. Representative images from patients with pathology that were acquired by the low-cost OCT and the Heidelberg Spectralis systems. *Scale bars*: 500 μm.

Downloaded from abstracts.iovs.org on 04/24/2024

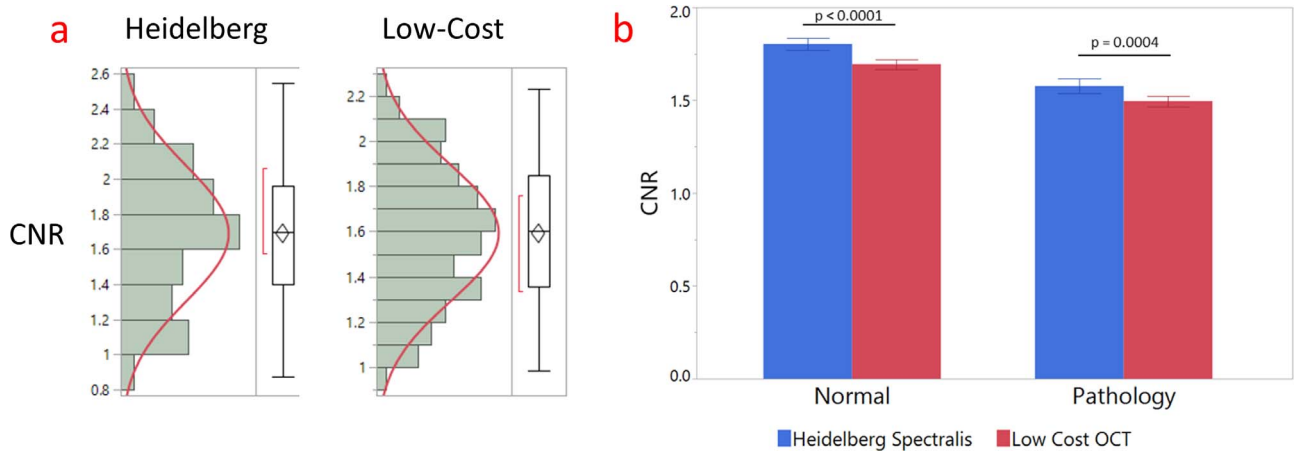

Figure 10. (a) CNR value distributions for the Heidelberg and low-cost OCT. (b) Mean CNR values for the Heidelberg and low-cost OCT differentiated by normal and pathology groups. Error bars indicate standard error of the mean (Std Error).

two imaging conditions on the same patients. We found no significant difference in mean CNR between images acquired in handheld mode and those acquired using a chin rest ($n = 20$, five patients, two eyes in two directions each, $P > 0.05$).

Discussion

We have presented a new low-cost OCT system and compared its clinical imaging capability with a standard commercial OCT system. A clinical study of imaging human retina was completed, comprising 120 eyes of 60 patients imaged using both the low-cost OCT and the standard Heidelberg Spectralis OCT. The low-cost OCT clearly demonstrated an ability to resolve features and layers necessary for clinical diagnosis. Furthermore, through CNR measurements and comparisons of the images acquired from both systems, we showed that only a 5.6% mean difference in contrast-to-noise ratio was present between the two devices. Although the mean CNR values of the two instruments are statistically distinct, a 5.6% difference is not expected to have a practical impact on most diagnostic applications, especially considering that the low-cost OCT comes at a fraction of the cost of the higher performance system. Notably, the CNR standard deviation across images was 0.3 and 0.4 for the low-cost and Spectralis systems, respectively, indicating that patient-to-patient variability exceeds the small difference in the CNR metric. Moreover, handheld imaging was also performed using the low-cost OCT scanner. Resulting analysis showed no significant mean CNR difference between handheld imaging and imaging with a chin rest. This result supports our system's ability to conduct handheld clinical imaging, with the only possible drawback of a longer imaging time due to less stability. Regardless, the low-cost OCT offers the flexibility of both modes of imaging in a clinical setting, without sacrificing system portability.

Table 3. Statistical Distributions of CNR Values and Paired *t*-Test Result for Both Systems

Parameter	Low-Cost OCT	Heidelberg Spectralis
Mean CNR ± std error	1.592 ± 0.021	1.687 ± 0.027
95% Confidence interval	1.551–1.634	1.634–1.740
Range	0.984–2.232	0.877–2.546
Mean CNR difference ± std error	0.09 ± 0.02	
Paired *t*-test *P* value	<0.0001	

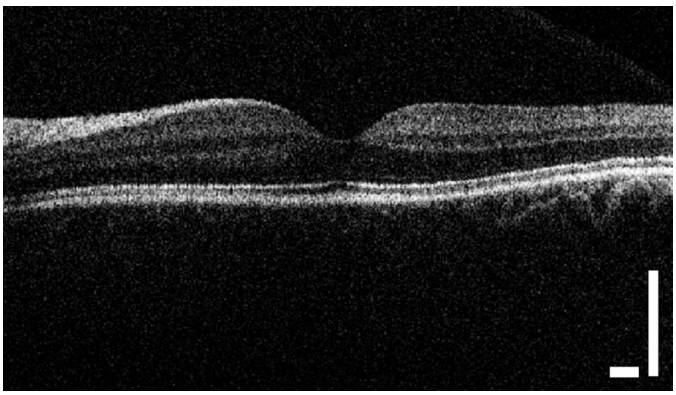

Figure 11. Representative image of a healthy retina acquired using the low-cost OCT in handheld mode. *Scale bar*: 500 μm.

Downloaded from abstracts.iovs.org on 04/24/2024

A current limitation of the low-cost system is power fluctuations of the SLD during imaging. The lower power stability results from the use of an open-loop cooling approach for the light source. This engineering step was made to keep cost down, but given the impact on the imaging signal from the retina, this will be resolved in future design iterations. Future development of the low-cost OCT system will include offering additional scanning patterns with the MEMS mirror. The current approach of only single vertical and horizontal line scan options limits application of the low-cost OCT system, particularly if there is pathology present off-center or away from the fovea. Raster or circular scanning patterns will overcome this limitation and can be implemented with a simple software change. Another future improvement will be to incorporate a fundus camera for en face imaging of the retina. The combination of these two complementing modalities will improve the localization of pathology on the retina. Finally, the system can be made to be entirely battery powered, further increasing portability. Currently, the system requires only 12 watts of power to function, meaning that the integrated PC can be replaced with a system on a module to permit transition to a fully battery-powered system.

Further development will be needed to commercialize the low-cost OCT system for routine clinical use. The cost estimate here compares the cost of materials of the low-cost system to the retail price of the Heidelberg Spectralis. The costs of commercial development, regulatory approval, and quality manufacturing processes will result in a higher final retail price of the low-cost system; however, this will also be offset by economies of scale in mass producing larger numbers of instruments. An estimated retail price of $10,000 to $20,000 for a commercial low-cost system will still provide a significantly lower cost than other commercial systems. Adoption of the low-cost OCT will require future clinical studies to further define its utility. However, the introduction of a low-cost OCT device offers great promise in improving access to retinal screening and early disease detection, especially in underserved areas and for vulnerable minority populations.

Acknowledgments

The authors thank the imaging team at the UNC Kittner Eye Center for their help in coordinating the clinical study. In particular, the authors thank Elizabeth Dubose, Sarah Armstrong, Debra Cantrell, Sean Grout, and Teesha Nicole Corcoran for their support.

Supported by National Institutes of Health (NIH) (R01 CA210544) and the Duke-Coulter Translational Partnership.

Disclosure: **G. Song**, None; **K.K. Chu**, None; **S. Kim**, None; **M. Crose**, Lumedica Inc. (I, E, C) P; **B. Cox**, Lumedica, Inc. (C); **E.T. Jelly**, None; **J.N. Ulrich**, None; **A. Wax**, Lumedica, Inc. (I, C, S) P

References

1. Adhi M, Duker JS, Optical coherence tomography–current and future applications. *Curr Opin Ophthalmol*. 2013;24:213–221.
2. Schmidt-Erfurth U, Klimscha S, Waldstein SM, Bogunović H. A view of the current and future role of optical coherence tomography in the management of age-related macular degeneration. *Eye*. 2016;31:26.
3. Garg S, Davis RM. Diabetic retinopathy screening update. *Clin Diabetes*. 2009;27:140.
4. Monroy GL, Won J, Spillman DR, Dsouza R, Boppart SA. Clinical translation of handheld optical coherence tomography: practical considerations and recent advancements. *Journal Biomed Opt*. 2017;22:1–30.
5. Yang J, Liu L, Campbell JP, Huang D, Liu G. Handheld optical coherence tomography angiography. *Biomed Opt Express*. 2017;8:2287–2300.
6. Liu X, Zaki FR, Wu H, Wang C, Wang Y. Temporally and spatially adaptive Doppler analysis for robust handheld optical coherence elastography. *Biomed Opt Express*. 2018;9:3335–3353.
7. Larocca F, Nankivil D, Farsiu S, Izatt JA. Handheld simultaneous scanning laser ophthalmoscopy and optical coherence tomography system. *Biomed Opt Express*. 2013;4:2307–2321.
8. Jung W, Kim J, Jeon M, et al. Handheld optical coherence tomography scanner for primary care diagnostics. *IEEE Trans Biomed Eng*. 2011;58:741–744.
9. Sayegh SI, Nolan RM, Jung W, et al. Comparison of a MEMS-based handheld OCT scanner with a commercial desktop OCT system for retinal evaluation. *Trans Vis Sci Tech*. 2014;3:10–10.

Downloaded from abstracts.iovs.org on 04/24/2024

10. Demian D, Duma V-F, Sinescu C, et al. Design and testing of prototype handheld scanning probes for optical coherence tomography. *Proc Inst Mech Eng H*. 2014;228:743–753.
11. National Center for Chronic Disease Prevention and Health Promotion. *National Diabetes Statistics Report: Estimates of Diabetes and Its Burden in the United States*. 2014. Available at: https://www.cdc.gov/diabetes/pdfs/data/2014-report-estimates-of-diabetes-and-its-burden-in-the-united-states.pdf. Accessed February 17, 2019.
12. Zhang X, Saaddine JB, Chou C-F, et al. Prevalence of diabetic retinopathy in the United States, 2005–2008. *JAMA*. 2010;304:649–656.
13. American Academy of Ophthalmology Panel. *Preferred Practice Pattern Guidelines. Diabetic Retinopathy*. 2012. Available at: https://www.aao.org/preferred-practice-pattern/diabetic-retinopathy-ppp-updated-2017. Accessed February 17, 2019.
14. Optometric Clinical Practice Guideline. *Care of the Patient with Diabetes Mellitus, Reference Guide for Clinicians*. 2009. Available from: https://www.aoa.org/documents/optometrists/CPG-3.pdf. Accessed February 17, 2019.
15. Benoit SR, Swenor B, Geiss LS, Gregg EW, Saaddine JB. Eye care utilization among insured people with diabetes, U.S. 2010–2014. *Diabetes Care*. 2019;42:427–433.
16. Paz SH, Varma R, Klein R, Wu J, Azen SP. Noncompliance with vision care guidelines in Latinos with type 2 diabetes mellitus: The Los Angeles Latino Eye Study. *Ophthalmology*. 2006;113:1372–1377.
17. MacLennan PA, McGwin G Jr, Heckemeyer C, et al. Eye care use among a high-risk diabetic population seen in a public hospital's clinics. *JAMA Ophthalmol*. 2014;132:162–167.
18. Baker RS, Watkins NL, Wilson MR, Bazargan M, Flowers CW. Demographic and clinical characteristics of patients with diabetes presenting to an urban public hospital ophthalmology clinic. *Ophthalmology*. 1998;105:1373–1379.
19. Olayiwola JN, Sobieraj DM, Kulowski K, St. Hilaire D, Huang JJ. Improving diabetic retinopathy screening through a statewide telemedicine program at a large federally qualified health center. *J Health Care Poor Underserved*. 2011;22:804–816.
20. Shelton RL, Jung W, Sayegh SI, et al. Optical coherence tomography for advanced screening in the primary care office. *J Biophotonics*. 2014;7:525–533.
21. Kim S, Crose M, Eldridge WJ, et al. Design and implementation of a low-cost, portable OCT system. *Biomed Opt Express*. 2018;9:1232–1243.
22. Wojtkowski M, Srinivasan V, Ko T, et al. Ultrahigh-resolution, high-speed, Fourier domain optical coherence tomography and methods for dispersion compensation. *Opt Express*. 2004;12:2404–2422.
23. Zhao Y, Chu KK, Eldridge WJ, et al. Real-time speckle reduction in optical coherence tomography using the dual window method. *Biomed Opt Express*. 2018;9:616–622.
24. Szkulmowski M, Wojtkowski M. Averaging techniques for OCT imaging. *Opt Express*. 2013;21:9757–9773.

Downloaded from abstracts.iovs.org on 04/24/2024